A Novel Approach to Marine Wind Speed Assessment Using Synthetic Aperture Radar

TODD D. SIKORA

Department of Earth Sciences, Millersville University, Millersville, Pennsylvania

GEORGE S. YOUNG

Department of Meteorology, The Pennsylvania State University, University Park, Pennsylvania

NATHANIEL S. WINSTEAD

Applied Physics Laboratory, The Johns Hopkins University, Laurel, Maryland

(Manuscript received 18 April 2005, in final form 19 July 2005)

ABSTRACT

This paper describes a product that allows one to assess the lower and upper bounds on synthetic aperture radar (SAR)-based marine wind speed. The SAR-based wind speed fields of the current research are generated using scatterometry techniques and, thus, depend on a priori knowledge of the wind direction field. The assessment product described here consists of a pair of wind speed images bounding the wind speed range consistent with the observed SAR data. The minimum wind speed field is generated by setting the wind direction field to be directly opposite to the radar look direction. The maximum wind speed field is generated by setting the wind direction field to be perpendicular to the radar look direction. Although the assessment product could be generated using any marine SAR scene, it is expected to be most useful in coastal regions where the large concentration of maritime operations requires accurate, high-resolution wind speed data and when uncertainty in the a priori knowledge of the wind direction precludes the generation of accurate SAR-based wind speed fields. The assessment product is demonstrated using a case in the northern Gulf of Alaska where synoptic-scale and mesoscale meteorological events coexist. The corresponding range of possible SAR-based wind speed is large enough to have operational significance to mariners and weather forecasters. It is recommended that the product become available to the public through an appropriate government outlet.

1. Introduction

Adverse weather poses a great threat to mariners. For example, the United States Department of the Interior, Minerals Management Service, Alaska Outer Continental Shelf Region reports 26 weather-related coastal Alaskan shipwrecks between 1990 and 2000 inclusive (see information online at http://www.mms.gov/alaska/ref/ships/index.htm and search by cause using the keywords “weather” and “wind”).

Given the sparse in situ data network in most marine regions, mariners and operational weather forecasters have relied heavily on remotely sensed data in order to assess the state of marine meteorological conditions, including the near-surface wind vector. As evidence of this reliance, note that the National Data Buoy Center (NDBC) provides Internet links to the latest space-borne scatterometer wind vector fields (10 m above sea level and neutral static stability) in the vicinity of its dedicated surface observation stations (see the Web site http://www.ndbc.noaa.gov). Scatterometers operate on the premise that the microwave normalized radar cross section (NRCS) of the ocean surface is related to the wind vector (e.g., Stoffelen and Anderson 1997). Typical scatterometers have order of magnitude 10 km

Corresponding author address: Todd D. Sikora, Dept. of Earth Sciences, Millersville University, Millersville, PA 17551.
E-mail: Todd.Sikora@millersville.edu

resolution and land contamination precludes their use in a resolution-size band directly adjacent to the shore.

Recent research has proven that NRCS from spaceborne synthetic aperture radar (SAR) can be used to produce marine wind speed fields[1] that are comparable to those provided by scatterometers (e.g., Horstmann et al. 2003; Monaldo et al. 2004a). The resolution of SAR is several orders of magnitude higher than that of scatterometers. Thus, SAR has the potential to provide detail in wind speed fields beyond that available from scatterometers and to provide coastal wind speed fields where scatterometers fail. This type of high-resolution (order of magnitude 0.1–1 km) SAR-based wind speed data is being produced and archived at The Johns Hopkins University Applied Physics Laboratory's Ocean Remote Sensing Group (JHUAPL) under the auspices of the Alaska SAR Demonstration (Monaldo 2000) (online at http://fermi.jhuapl.edu/sar/stormwatch/web_wind/).

A major obstacle to SAR-based wind speed retrieval is the requirement for a priori knowledge of the wind direction. This problem is made evident in the general form of the geophysical model function (GMF) relating NRCS to wind speed:

$$\sigma_0 = A(\theta)U^{\gamma(\theta)}[1 + B(\theta, U)\cos\varphi + C(\theta, U)\cos 2\varphi]. \tag{1}$$

Here, σ_0 is NRCS, U is wind speed, φ is the relative angle between the wind direction and the radar look direction, θ is the local radar incident angle, and A, B, C, and γ are parameters that depend on incident angle and wind speed. Thus, the inversion is not unique because at moderate incident angles and wind speeds, any one value of NRCS can correspond to several wind speed–wind direction pairs. Scatterometers reduce this uncertainty by sensing a given area of ocean surface with multiple antennas.

Researchers aiming to produce SAR-based wind speed fields have employed a variety of techniques to ascertain the wind direction field coincident with SAR imagery. For example, scatterometer wind directions have been used by Monaldo et al. (2004a). Numerical model wind directions have been used by Monaldo et al. (2001). And, the SAR signatures of linear geophysical features assumed to be aligned with the wind direction [e.g., atmospheric roll vortices; Alpers and Brümmer (1994)] have been employed by Horstmann et al. (2000).

[1] Monaldo et al. (2004b) provides a review of the current suite of SAR wind retrieval techniques. Our research focuses solely on the scatterometry approach.

Each of the above-mentioned wind direction estimation techniques has potential shortcomings, especially in coastal regions. As mentioned earlier, scatterometer wind data have a much coarser resolution than SAR data and are not available close to coastlines.

Operational numerical model data are typically at least as coarse as scatterometer data and mesoscale and microscale interpretations of such data are often suspect. For example, we have found that it is not uncommon for synoptic-scale fronts and cyclones to be displaced by mesoscale distances with respect to their signatures in corresponding SAR imagery (e.g., Young et al. 2005). Moreover, in the vicinity of complex coastlines, model data become questionable because of the difficulty in fully resolving the terrain and its impact on the mesoscale flow (Mass et al. 2002).

Finally, linear features may be absent in SAR images or, if present, may not be aligned with the wind direction. For example, one may mistake the SAR signature of atmospheric gravity waves for atmospheric roll vortices. [Winstead et al. (2002) provides SAR examples of coincident atmospheric gravity waves and roll vortices over Lake Superior.] This problem is acute in the vicinity of coastlines because topographically forced gravity waves are more common in those regions than over the open ocean.

The objective of this paper is to propose a product that allows one to assess the lower and upper bounds on SAR-based wind speed. Although this product could be generated for any marine SAR scene, we envision it to be most useful in coastal regions where the large concentration of maritime operations requires accurate, high-resolution wind speed data and when the above-mentioned wind direction uncertainties preclude the generation of accurate SAR-based wind speed data.

2. Methodology

For the sake of brevity, we will focus on a wind speed assessment product based on ScanSAR Wide data (processed at the Alaska SAR Facility) from the SAR on board the Canadian Space Agency's *RADARSAT-1*. That SAR is C-band (5.6 cm) and right looking with horizontal–horizontal polarization. We generate our SAR-based wind speed fields following the methodology outlined in section II of Monaldo et al. (2004a). In particular, we use the GMF known as CMOD4 (Stoffelen and Anderson 1997) modified for horizontal–horizontal polarization using a polarization parameter of 0.6.

We note that ongoing research is investigating the robustness of other GMFs (e.g., CMOD5; Hersbach

2003) and polarization parameters (Monaldo et al. 2004b). In fact, as of the time of this writing, JHUAPL is transitioning from the use of CMOD4 to the use of CMOD5. The product we describe herein is designed so that it can be generated using any scatterometry approach for producing SAR-based wind speed data, thereby allowing easy conversion to the most appropriate GMF. Given that, and the fact that we have more complete information on the physical limits of CMOD4[2] than the newer CMOD5, we choose to present our product based on CMOD4.

To produce our wind speed assessment product, we generate two SAR-based wind speed images. One image is generated using a value of φ corresponding to a wind direction opposite to the radar look direction (φ = 000°, 360°). The other image is generated using a value of φ corresponding to a wind direction perpendicular to the radar look direction (φ = 090°, 270°). For a given value of NRCS, φ = 000°, 360° produces the minimum value of wind speed and φ = 090°, 270° produces the maximum value of wind speed for moderate incident angles and wind speed conditions. The pixel size is a tunable parameter. For the current research, we have followed JHUAPL's choice of 600-m pixels for their online ScanSAR Wide SAR-based wind speed data.

Thus, two assessment images are produced. One image shows the minimum possible SAR-based wind speed on a pixel-by-pixel basis and the other shows the maximum possible SAR-based wind speed on a pixel-by-pixel basis. Together, these two images provide the lower and upper bounds on the SAR-based wind speed field, suitable for use in maritime operations and forecasting.

To provide the reader with a conventional estimate of SAR-based wind speed field in the case study presented below, we show a SAR-based wind speed image using a wind direction field from the U.S. Navy's Operational Global Atmospheric Prediction System (NOGAPS) model. This is the primary wind direction technique used at JHUAPL for the production of their online SAR-based wind speed data. In doing so, we will identify several likely areas of wind direction error by NOGAPS.

[2] SAR-based wind speed data generated using CMOD4 become questionable at large values of true wind speed (Donnelly et al. 1999) where the CMOD4 GMF tends to underestimate the true wind speed. We have chosen to saturate our bounds images at 25.0 m s^{-1}, following the methodology JHUAPL uses for their online ScanSAR Wide SAR-based wind speed data generated using CMOD4.

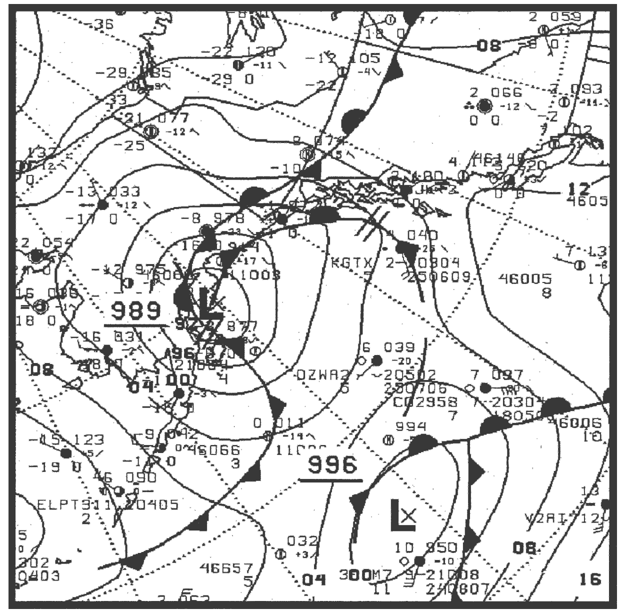

FIG. 1. Surface analysis from NCEP for 0000 UTC 18 Feb 2000. A synoptic-scale cyclone is analyzed over the northwest Gulf of Alaska with a surface front extending east and then southeastward near the Alaskan coast.

3. Case study

a. Meteorological setting

To illustrate the utility of our approach to SAR-based wind speed assessment, we will demonstrate our procedure on a case involving coincident synoptic-scale and mesoscale marine meteorological events over the northern Gulf of Alaska. The SAR image for this case (not shown) was taken at 0310 UTC 18 February 2000. The corresponding surface synoptic analysis from the National Centers for Environmental Prediction (NCEP) is provided in Fig. 1. Figure 1 makes clear the challenges faced by anyone attempting to analyze the near-surface wind field in a data-sparse offshore region such as the Gulf of Alaska. The available coastal, ship, and buoy observations, coupled with conventional meteorological satellite data, are just sufficient to allow the analyst to determine that a strong synoptic-scale cyclone is present over the northern Gulf of Alaska and that some form of meteorological boundary extends in a general eastward direction from the cyclone's center, roughly paralleling the Alaskan coast. That boundary is depicted as an occluded front in Fig. 1 despite its location in the warm sector of the cyclone. As will be shown in the next subsection, that boundary is actually the seaward edge of a mesoscale barrier jet and thus is associated with a sharply defined band of markedly larger cyclonic winds directly adjacent to the coast (e.g., Overland and Bond 1993; Loescher et al. 2006).

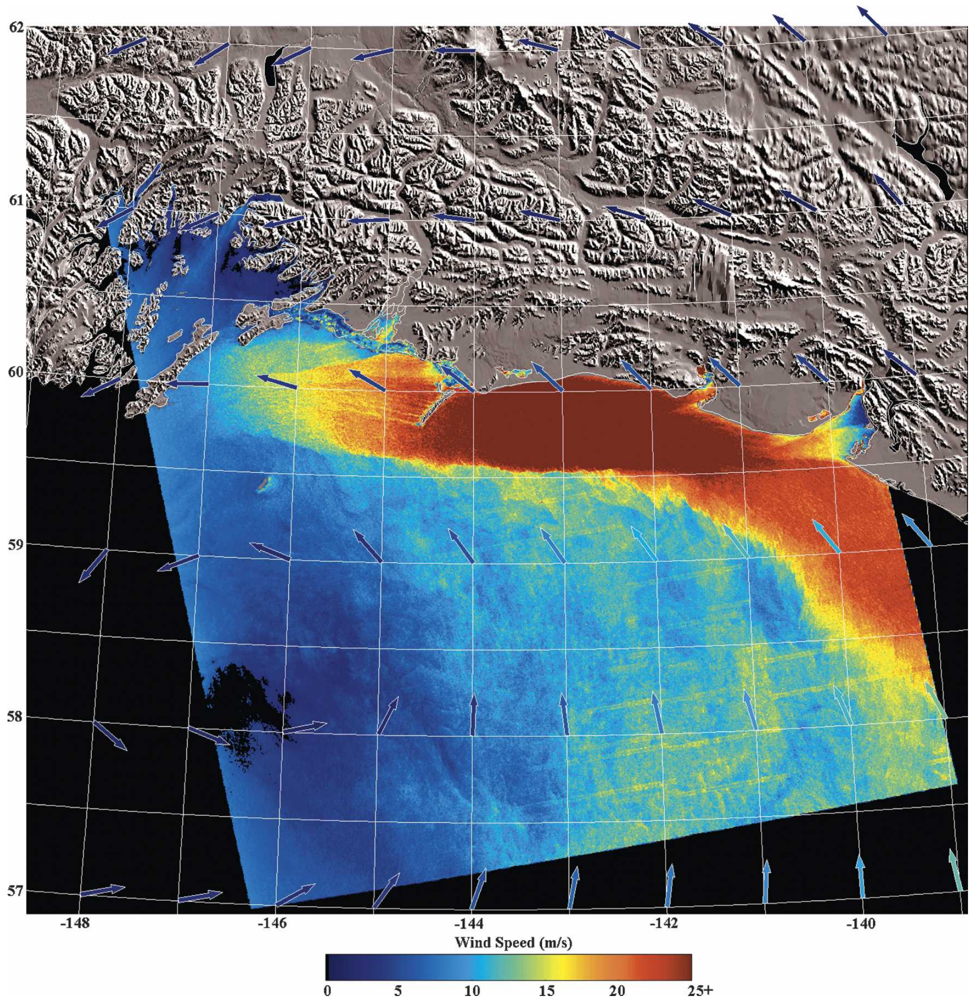

FIG. 2. SAR-based wind speed image of the northeast Gulf of Alaska at 0310 UTC 18 Feb 2000, based on the NOGAPS wind direction field.

b. *Results*

Here, we will illustrate the range of possible SAR-based wind speeds for this case study. The SAR-based wind speed field resulting from the use of NOGAPS wind directions is shown in Fig. 2. The colored arrows found at the latitude–longitude intersections in Fig. 2 represent the NOGAPS wind vector field. These NOGAPS wind vectors are 6-h forecasts from the model's 0000 UTC 18 February 2000 run. According to NOGAPS, a synoptic-scale cyclone is located to the west of the image. Analysis of the SAR image using the techniques provided in Young et al. (2005), however, indicates that the cyclone is actually centered at about 58.25°N, 146.50°W. According to NOGAPS, the cyclone is producing southerly and southeasterly flow toward the coast throughout most of the imaged area.

Notice that the resulting SAR-based wind speed is 5.0–15.0 m s^{-1} over most of the southwestern portion of the image, with the wind speed decreasing toward the cyclone's center. However, directly adjacent to the Alaskan coastline, a sharply defined 50-km-wide band of markedly larger wind speed is found. This band is a mesoscale barrier jet resulting from the interaction of the synoptic-scale flow with the coastal topography (Loescher et al. 2006). Although not resolved by NOGAPS, the likely wind direction within the barrier jet is cyclonic, mainly paralleling the shore (Overland and Bond 1993). Note that the SAR-based wind speed is $\geq$25.0 m s^{-1} over much of the jet's length. Of particular interest to mariners and operational weather forecasters is the sharp jump in wind speed along the seaward edge of the barrier jet. This jump occurs where the onshore flow due to the cyclone meets the shore-parallel flow within the barrier jet. Moreover, the wind speed image reveals smaller, 15.0–25.0 m s^{-1} gap flow

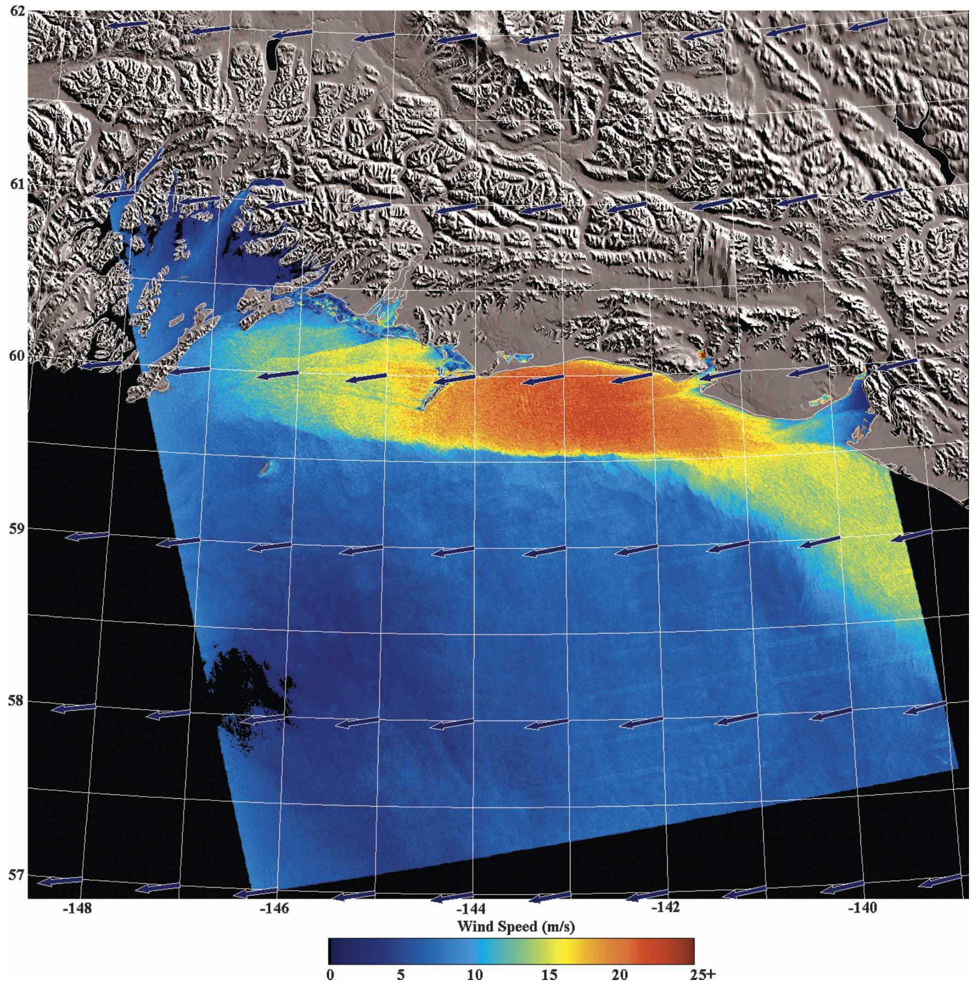

FIG. 3. SAR-based wind speed image of the northeast Gulf of Alaska at 0310 UTC 18 Feb 2000, based on an assumed wind direction field opposite to the radar look direction.

jets (e.g., Macklin et al. 1990) that appear, by their orientation, to feed out of the two bays near 60.00°N, 141.50°W (Icy Bay) and 59.75°N, 140.00°W (Yakutat Bay), and merge into the barrier jet. The likely gap flow wind directions are also not resolved by NOGAPS.

Recall that we have documented several likely areas of wind direction forecast error by NOGAPS for this case study. The range of possible SAR-based wind speeds that could result from the incorrect forecast of the wind direction can be seen by comparing Figs. 3 and 4. The blue arrows found at the latitude–longitude intersections in Figs. 3 and 4 represent the constant wind direction fields we impose (080° and 170° from true north, respectively). Figure 3 presents the minimum SAR-based wind speed field, that which would exist if the wind direction is everywhere opposite to the radar look direction. In contrast, Fig. 4 presents the maximum SAR-based wind speed field, that which would exist if the wind direction is everywhere perpendicular to the radar look direction. These two figures provide the lower and upper bounds on the wind speed field consistent with the SAR data.

As expected, the strength of the flow in Fig. 3 is greatly reduced from that in Fig. 4. For example, the wind speed of the eastern portion of the barrier jet decreases from $\geq$25.0 m s^{-1} to less than about 17.5 m s^{-1}, while that of the center portion of the barrier jet decreases from $\geq$25.0 m s^{-1} to less than about 20.0 m s^{-1}. As can be seen by comparing Figs. 2, 3, and 4, the SAR-based estimates of surface wind speed can lie anywhere in this range of direction-dependent possibilities. Where the true wind direction is mainly opposite to the radar look direction—as in the center portion of the barrier jet, the two gap flows, and that portion of the synoptic wind field north of the cyclone's center—the true wind speed will be near the lower limit. As

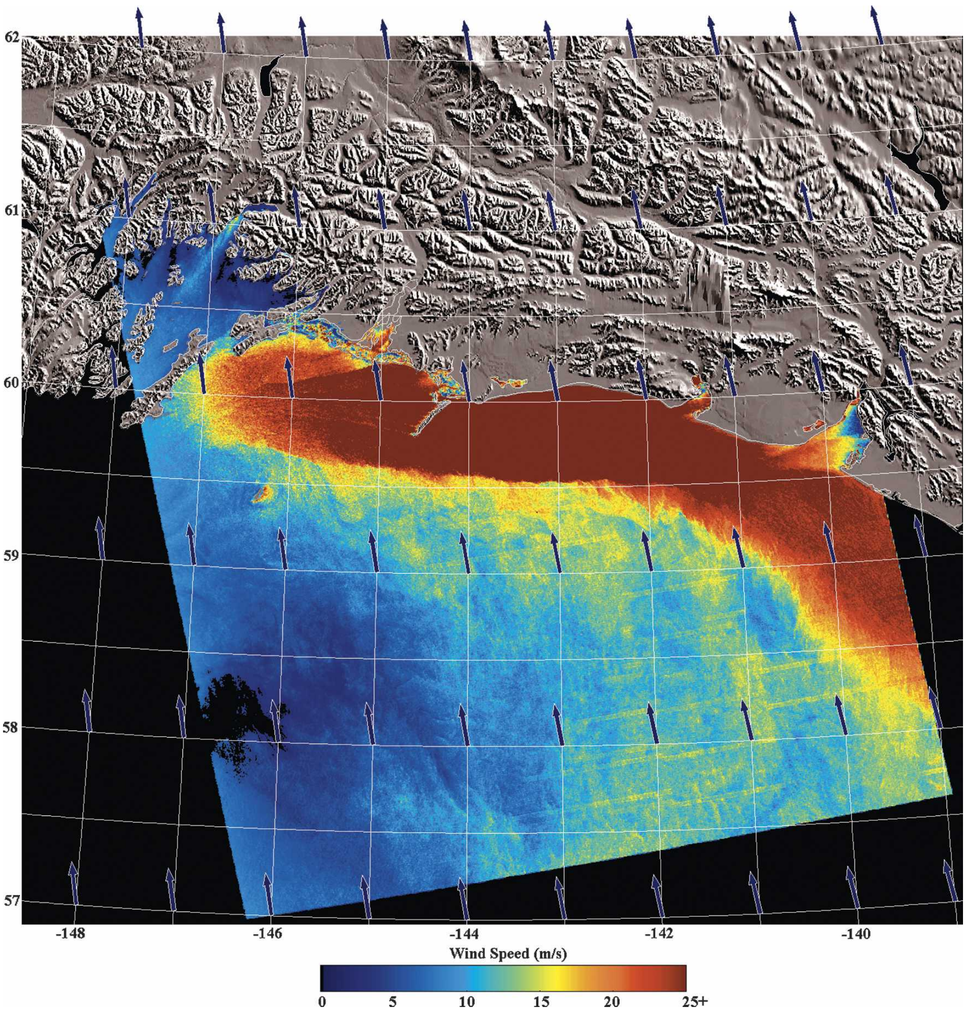

FIG. 4. SAR-based wind speed image of the northeast Gulf of Alaska at 0310 UTC 18 Feb 2000, based on an assumed wind direction field perpendicular to the radar look direction.

evidence of this, NDBC station 46061, located at 60.22°N, 146.83°W, reported a wind direction of 076° from true north and a wind speed of 10.8 m s^{-1} at 0300 UTC 18 February 2000, almost exactly matching the wind information found at 60.22°N, 146.83°W in Fig. 3. Where the wind direction is mainly perpendicular to the radar look direction—as in the eastern portion of the barrier jet and that portion of the synoptic wind field east of the cyclone's center—the true wind speed will be near the upper limit. Where reliable automated wind direction information is unavailable, prudence dictates one assume that the wind speeds depicted in Fig. 4 are at least possible.

4. Summary and recommendations

This paper describes and demonstrates a high-resolution (order of magnitude 0.1–1 km) wind speed assessment product based on SAR. The product allows one to assess the bounds on SAR-based wind speed, on a pixel-by-pixel basis, using scatterometry techniques. Simply put, the minimum SAR-based wind speed at each pixel is produced by setting the wind direction at each pixel to be opposite to the radar look direction. In contrast, the maximum SAR-based wind speed at each pixel is produced by setting the wind direction at each pixel to be perpendicular to the radar look direction.

We envision the assessment product to be most useful in coastal regions where the large concentration of maritime operations requires accurate, high-resolution wind speed data and when wind direction errors preclude the generation of accurate SAR-based wind speed data. Thus, we demonstrate the product using a case in the northern Gulf of Alaska where synoptic-scale and mesoscale meteorological events coexist. The range of possible SAR-based wind speeds in the demonstration is large enough to have operational significance to mariners and forecasters. Given that SAR-based wind speed fields can be produced within several hours of SAR image acquisition time, we recommend that our approach to SAR-based wind speed analysis become available to the public though an appropriate government outlet.

Acknowledgments. This research was supported by Office of Naval Research Grants N00014-04-WR20365, N00014-04-10539, and N00014-05-WR20319 as well as National Science Foundation Grant ATM-0240869. We thank Frank M. Monaldo and Donald R. Thompson for the technical assistance they provided in the preparation of this manuscript.

REFERENCES

Alpers, W., and B. Brümmer, 1994: Atmospheric boundary layer rolls observed by the synthetic aperture radar aboard the ERS-1 satellite. *J. Geophys. Res.,* **99,** 12 613–12 621.

Donnelly, W. J., J. R. Carswell, R. E. McIntosh, P. S. Chang, J. Wilderson, F. Marks, and P. G. Black, 1999: Revised ocean backscatter models at C and Ku band under high-wind conditions. *J. Geophys. Res.,* **104,** 11 485–11 497.

Hersbach, H., 2003: An improved geophysical model function for ERS C-band scatterometry. ECMWF Tech. Memo. 395, 50 pp.

Horstmann, J., W. Kock, S. Lehner, and R. Tonboe, 2000: Wind retrieval over the ocean using synthetic aperture radar with C-band HH polarization. *IEEE Trans. Geosci. Remote Sens.,* **38,** 2122–2131.

——, J. Schiller, J. Schulz-Stellenfleth, and S. Lehner, 2003: Global wind speed retrieval from SAR. *IEEE Trans. Geosci. Remote Sens.,* **41,** 2277–2286.

Loescher, K. A., G. S. Young, B. A. Colle, and N. S. Winstead, 2006: Climatology of barrier jets along the Alaskan coast. Part I: Spatial and temporal distribution. *Mon. Wea. Rev.,* **134,** 437–453.

Macklin, S. A., N. A. Bond, and J. P. Walker, 1990: Structure of a low-level jet over lower Cook Inlet, Alaska. *Mon. Wea. Rev.,* **118,** 2568–2578.

Mass, C., F. Mass, D. Ovens, K. Westrick, and B. A. Colle, 2002: Does increasing horizontal resolution produce more skillful forecasts? *Bull. Amer. Meteor. Soc.,* **83,** 407–430.

Monaldo, F., 2000: The Alaska SAR demonstration and near-real-time synthetic aperture winds. The Johns Hopkins University Technical Digest, Vol. 21, Applied Physics Laboratory, The Johns Hopkins University, Laurel, MD, 75–79.

——, D. R. Thompson, R. C. Beal, W. G. Pichel, and P. Clemente-Colón, 2001: Comparison of SAR-derived wind speed with model predictions and ocean buoy measurements. *IEEE Trans. Geosci. Remote Sens.,* **39,** 2587–2600.

——, ——, W. G. Pichel, and P. Clemente-Colón, 2004a: A systematic comparison of QuikSCAT and SAR ocean surface wind speeds. *IEEE Trans. Geosci. Remote Sens.,* **42,** 283–291.

——, and Coauthors, 2004b: The SAR measurement of ocean surface winds: An overview. SP-565, European Space Agency, 15–32.

Overland, J. E., and N. A. Bond, 1993: The influence of coastal orography: The Yakutat storm. *Mon. Wea. Rev.,* **121,** 1388–1397.

Stoffelen, A., and D. Anderson, 1997: Scatterometer data interpretation: Estimation and validation of the transfer function CMOD4. *J. Geophys. Res.,* **102,** 5767–5780.

Winstead, N. S., T. D. Sikora, D. R. Thompson, and P. D. Mourad, 2002: Direct influence of gravity waves on surface-layer stress during a cold air outbreak, as shown by synthetic aperture radar. *Mon. Wea. Rev.,* **130,** 2764–2776.

Young, G. S., T. D. Sikora, and N. S. Winstead, 2005: Use of synthetic aperture radar in finescale surface analysis of synoptic-scale fronts at sea. *Wea. Forecasting,* **20,** 311–327.